Structure of the Catalytic Domain of Human Polo-like Kinase 1[†,‡]

Michael Kothe,[§,||] Darcy Kohls,[§,||] Simon Low,[§,||] Rocco Coli,[§] Alan C. Cheng,[§] Suzanne L. Jacques,[§] Theresa L. Johnson,[§] Cristina Lewis,[⊥] Christine Loh,[§] Jim Nonomiya,[⊥] Alissa L. Sheils,[§] Kimberly A. Verdries,[§] Thomas A. Wynn,[§] Cyrille Kuhn,[§] and Yuan-Hua Ding*[,§]

Pfizer Global Research and Development, Research Technology Center, 620 Memorial Drive, Cambridge, Massachusetts 02139, and Pfizer Global Research and Development, La Jolla Laboratories, La Jolla California 92121

Received November 30, 2006; Revised Manuscript Received February 23, 2007

ABSTRACT: Polo-like kinase 1 (Plk1) is an attractive target for the development of anticancer agents due to its importance in regulating cell-cycle progression. Overexpression of Plk1 has been detected in a variety of cancers, and expression levels often correlate with poor prognosis. Despite high interest in Plk1-targeted therapeutics, there is currently no structure publicly available to guide structure-based drug design of specific inhibitors. We determined the crystal structures of the T210V mutant of the kinase domain of human Plk1 complexed with the nonhydrolyzable ATP analogue adenylylimidodiphosphate (AMPPNP) or the pyrrolo-pyrazole inhibitor PHA-680626 at 2.4 and 2.1 Å resolution, respectively. Plk1 adopts the typical kinase domain fold and crystallized in a conformation resembling the active state of other kinases. Comparison of the kinetic parameters determined for the (unphosphorylated) wild-type enzyme, as well as the T210V and T210D mutants, shows that the mutations primarily affect the k_{cat} of the reaction, with little change in the apparent K_m for the protein or nucleotide substrates (k_{cat} = 0.0094, 0.0376, and 0.0049 s^{-1} and $K_{m(ATP)}$ = 3.2, 4.0, and 3.0 μM for WT, T210D, and T210V, respectively). The structure highlights features of the active site that can be exploited to obtain Plk1-specific inhibitors with selectivity over other kinases and Plk isoforms. These include the presence of a phenylalanine at the bottom of the ATP pocket, combined with a cysteine (as opposed to the more commonly found leucine) in the roof of the binding site, a pocket created by Leu132 in the hinge region, and a cluster of positively charged residues in the solvent-exposed area outside of the adenine pocket adjacent to the hinge region.

Polo-like kinase 1 (Plk1)[1] is an important component of the cell-cycle control machinery and plays key roles during the G2/M transition through phosphorylation of substrates that have functions in mitosis and need to be regulated in a cell-cycle-dependent manner (*1*−*3*). Plk1 is highly expressed in proliferating cells and overexpressed in many cancers, where expression levels often correlate with poor prognosis (*4*−*11*). Downregulation of Plk1 expression causes reduced proliferation in a variety of cancer cell lines and tumor xenografts (*12*−*16*), while it shows no effect on the viability of untransformed cells (*15*, *16*). As such, Plk1 represents an attractive target for the development of anticancer agents. Both clinical and experimental data have indicated that Plk1 dysregulation leads to cancer and that inhibiting aberrant Plk1 activity might offer a new approach for cancer therapy. A high-resolution crystal structure would enable the rational design of potent and selective Plk1 inhibitors with potential as cancer therapeutics.

Polo-like kinases are defined by the presence of one or two polo-boxes of approximately 80 residues in length in their peptide sequence. In mammals, four Plks have been identified: Plk1, Plk2 (Snk), Plk3 (Fnk or Prk), and Plk4 (Sak). Of these, Plk1 is the best characterized and has the highest degree of homology to the single Plk gene in lower organisms. It is believed to carry out most of the conserved Plk functions during mitosis and cytokinesis, while the other members are believed to have more specialized and less well characterized roles. All family members contain an N-terminal kinase domain and a C-terminal polo-box domain (PBD) composed of either one (Plk4) or two polo-boxes.

[†] Use of the IMCA-CAT beamlines 17-ID and 17-BM at the Advanced Photon Source was supported by the companies of the Industrial Macromolecular Crystallography Association through a contract with the Center for Advanced Radiation Sources at the University of Chicago. Use of the Advanced Photon Source was supported by the U. S. Department of Energy, Office of Science, Office of Basic Energy Sciences, under Contract No. W-31-109-Eng-38.

[‡] Atomic coordinates have been deposited in the Protein Data Bank as entries 2OU7 (AMPPNP complex) and 2OWB (PHA-680626 complex).

* Corresponding author. Tel. (617) 551-3168. Fax. (617) 551-3178. E-mail: yuan-hua.ding@pfizer.com.

[||] These authors contributed equally to this work.

[§] Pfizer Global Research and Development, Research Technology Center.

[⊥] Pfizer Global Research and Development, La Jolla Laboratories. Current address: Genentech, Inc., South San Francisco, CA 94080.

[1] Abbreviations: ABL, Abelson tyrosine kinase; AMPPNP, adenylylimidodiphosphate; CDK2, cyclin-dependent kinase 2; CHK1, checkpoint kinase 1; EGFR1, epidermal growth factor receptor 1; FGFR1, fibroblast growth factor receptor 1; Fnk, fibroblast-growth-factor-inducible kinase; GSK3β, glycogen synthase kinase 3 beta; IRK, insulin receptor kinase; LCK, lymphocyte-specific protein kinase; LYN, v-yes-1 Yamaguchi sarcoma viral related oncogene homologue; MYT1, myelin transcription factor 1. PBD, Polo-box domain; PI3K, phosphoinositide-3-kinase; PKA, protein kinase A; PKC, protein kinase C; Plk, polo-like kinase; Prk, proliferation-related kinase; Sak, Snk akin kinase; Snk, serum-inducible kinase; VEGFR3, vascular endothelial growth factor receptor 3.

10.1021/bi602474j CCC: $37.00
Published on Web 04/27/2007

The Plk1 PBD crystal structure (residues 367−603) has been solved (*17*, *18*) and shown to constitute a single phosphopeptide-binding domain formed by the two polo-boxes serving as symmetrical halves with the phosphopeptide binding in a groove between the two polo-boxes. The PBD has been implicated in Plk localization through interaction with phosphorylated scaffolding proteins or Plk substrates (*19*, *20*) and in autoinhibition of Plk1 activity in the absence of PBD binding partners (*21*, *22*).

Plk isoforms are regulated throughout the cell cycle (*23*−*25*) by changes in expression levels, by localization mediated through the PBD domain (*19*, *20*), and by phosphorylation of at least one residue in the kinase domain (*26*−*29*). Phosphorylation of Thr210 in the activation loop increases Plk1 activity and is thought, by analogy to other protein kinases, to result in stabilization of the activation loop in a conformation in which important active site residues are properly positioned for substrate binding and catalytic activity (*30*). A second residue implicated in Plk1 activation is Ser137 (*28*, *29*), whose function is less understood. Mutation of either of these residues to aspartate to mimic the phosphorylated state results in increased Plk1 activity, and mutation of Thr210 to valine reduces activity relative to wild-type.

Several inhibitors of Plk1 activity have been reported to date (*3*, *31*). The natural product scytonemin inhibits Plk1 with an IC_{50} of 2 μM but is nonselective, inhibiting myelin transcription factor 1 (MYT1), cyclin-dependent kinase 1 (CDK1), checkpoint kinase 1 (CHK1), and protein kinase C (PKC) with similar potencies (*32*). The cyclin-dependent kinase 2 (CDK2) inhibitor purvalanol A also inhibits Plk1 with micromolar potency (*31*). The phosphatidylinositide-3 (PI3) kinase inhibitor wortmannin was found to inhibit Plk1 with an IC_{50} value of 24 nM (*33*), most likely by covalent modification through interaction with the conserved Lys82 in a manner analogous to its mode of action against phosphoinositide-3-kinase (PI3K) (*34*). However, selective and potent ATP-competitive inhibitors of Plk1 are achievable, as indicated by the dihydropteridinone derivative BI 2536 (*35*−*37*). This compound has been reported to be a selective inhibitor of Plk1 with sub-nanomolar potency and is currently undergoing Phase I clinical trials. Several other pharmaceutical companies have also disclosed ATP-competitive Plk1 inhibitors (*38*−*41*).

Despite the high interest in Plk1 as a potential drug target, the crystal structure of this key mitotic enzyme has not yet been reported in the literature. To facilitate the design and optimization of ATP-competitive Plk1 inhibitors, we have determined the structures of the Plk1 kinase domain T210V mutant complexed with the nonhydrolyzable ATP analogue adenylylimidodiphosphate (AMPPNP) and also with the pyrrolo-pyrazole inhibitor PHA-680626 (*42*) at 2.4 and 2.1 Å resolution, respectively. PHA-680626 was originally reported as an inhibitor of Aurora A kinase, but we found that it also inhibits Plk1 with sub-micromolar potency. The structures reported here represent the first examples of crystal structures of the kinase domain of a member of the clinically important Plk family. Plk1 adopts the classical kinase fold with the ligands showing the expected interactions with the protein in the cleft between the N- and the C-terminal lobes. Analysis of the structure provides insights into residues that are likely to contribute to potency and specificity and which may present opportunities for the design of selective Plk1 inhibitors.

EXPERIMENTAL METHODS

Cloning, Protein Expression, and Purification. All constructs contained an N-terminal hexahistidine tag followed by a PreScission protease cleavage site and were cloned into pFastBac1 (Invitrogen, Carlsbad, CA). Recombinant Plk1 proteins were expressed in *Spodoptera frugiperda* (Sf21) insect cells using Wave Bioreactors (Wave Biotech, Somerset, NJ) and SF-900 II serum-free media (Invitrogen) using a TIPS protocol (*43*). For purification, cell paste was resuspended in (50 mL per liter of cell paste) ice-cold lysis buffer (50 mM HEPES pH 7.5, 500 mM NaCl, 50 mM imidazole, 5 mM Tris (2-carboxyethyl) phosphine hydrochloride (TCEP), plus protease inhibitors) and lysed by single passage through a prechilled microfluidizer (M110L, Microfluidics International Corp., Needham, MA) at 18 kPSI chamber pressure. Lysate was centrifuged overnight at 41000*g* at 4 °C. All subsequent purification steps were conducted at 4 °C. The supernatant was decanted and passed through an Amersham HiTrap nickel chelating affinity column. After washes with lysis buffer, followed by 50 mM HEPES pH 7.5, 500 mM NaCl, 5 mM TCEP, 100 mM imidazole, bound protein was eluted by increasing the imidazole concentration to 200 mM. The eluate was dialyzed against 50 mM HEPES pH 7.5, 5 mM TCEP and then treated overnight with PreScission protease (Amersham) at 4 °C. The PreScission-treated protein was passed through a second Amersham HiTrap nickel chelating affinity column to remove any remaining affinity-tagged protein. The cleaved protein bound nonspecifically to the column and was eluted with 75 mM imidazole, pooled and concentrated, and passed over an Amersham Superdex 200 gel filtration column equilibrated with 50 mM HEPES pH 7.5, 5 mM TCEP. The eluted protein was concentrated to 25−35 mg/mL, flash frozen in liquid nitrogen, and stored at −80 °C until further use. Proteins expressed from all three constructs were confirmed to be unphosphorylated by electrospray mass spectroscopy analysis (data not shown).

Full-length CDC25c was expressed as inclusion bodies in *Escherichia coli*. The inclusion bodies were suspended with 1 mL/g of suspension buffer (25 mM Tris HCl pH 8.0, 0.5 M NaCl, 5 mM DTT) and homogenized. An equal volume of denaturation buffer (25 mM Tris HCl pH 8.0, 0.5 M NaCl, 5 mM DTT, 8 M urea) was added followed by incubation for 20 min at 40 °C. The suspension was centrifuged at 30000*g* for 20 min. The supernatant was collected and diluted to a final concentration of 1 mg/mL with dilution buffer (25 mM Tris HCl pH 8.0, 0.5 M NaCl, 5 mM DTT, 8 M urea). The protein was refolded by sequential dialyzing against 6, 2, and 0 M urea in 25 mM Tris HCl pH 8.0, 0.5 M NaCl, 5 mM DTT. Insoluble material was removed by centrifugation at 42000*g*.

Crystallization. Initial crystals were obtained at 4 °C in Topaz screening chips (*44*) (Fluidigm, South San Francisco) with the T210V mutant at 12 mg/mL in 50 mM HEPES, pH 7.5, 5 mM TCEP and using 0.1 M Tris, pH 8.5, 0.4 M sodium malonate, 18% PEG 4000 or 0.1 M sodium citrate, pH 5.6, 0.6 M magnesium acetate, 18% PEG 4000 as crystallization buffer. Crystals were obtained by the hanging

drop method using Plk1 (T210V) at 12 mg/mL in 50 mM HEPES, pH 7.5, 5 mM TCEP. Protein was incubated on ice with 5 mM ligand (1:20 dilution of 100 mM stock in H_2O for AMPPNP or DMSO for PHA-680626) for 0.5−1 h, followed by a brief centrifugation step and drop setting at RT (0.5 μL of protein + 0.5 μL of reservoir solution consisting of 500 mM magnesium acetate, 10% PEG 4000, and 0.3 mM zinc acetate for AMPPNP, and 350 mM sodium malonate, 15% PEG 4000, and 0.6 mM zinc acetate for PHA-680626). Crystal trays were incubated at 4 °C. With the exception of zinc acetate, which was from Hampton Research (Aliso Viejo, CA), all reservoir components were from Fluidigm. Crystals appeared overnight and continued to grow over several days to dimensions of up to 0.5 × 0.1 mm. Crystals were frozen after 1 min incubation in a 1:1 mixture of cryoprotecting and reservoir solutions, followed by a 1 min incubation in 100% cryoprotecting solution. The cryoprotecting solution consisted of 1 mM ligand in 25% glycerol, 0.5 mM Zn acetate, and (1) 0.7 M Mg acetate, 11% PEG 4000, 6.5 mM HEPES, pH 7.5, and 0.65 mM TCEP for AMPPNP, or (2) 0.3 M Na malonate, 15% PEG 4000, 12.5 mM HEPES, pH 7.5, and 1.25 mM TCEP for PHA-680626.

Data Collection, Structure Determination, and Refinement. The AMPPNP and PHA-680626 Plk1 datasets were collected at the Advanced Photon Source (Argonne National Laboratories) at the IMCA-CAT Beamlines 17-ID and 17-BM, respectively. Data were scaled and integrated using HKL2000 (*45*). The initial structure was solved by molecular replacement with Molrep from the CCP4 package (*46*). The structure of Aurora A protein kinase (PDB: 1MQ4) with the activation loop (residues 274−307) deleted was used as a search model due to the high level of sequence similarity with Plk1. Crystals belong to the space group $P3_221$ with one molecule in the asymmetric unit. A solution was found with initial *R* factor of 0.59 and correlation coefficient of 0.246. The initial electron density map was of sufficient quality for initial model building including the region that was omitted. Model building proceeded with successive iterations of TLS refinement with Refmac 5 (*47*) and manual rebuilding with the program Quanta (Accelrys) (*48*). All data and statistics are presented in Table 1. The models consist of one uninterrupted chain with density observed for residues 37−330 and 37−328 for the PHA-680626 and AMPPNP structures, respectively.

Kinase Activity Assays. Plk1 activity was measured using recombinant Cdc25c (expressed in *E. coli* and refolded from inclusion bodies) as substrate. Assay buffer consisted of 10 mM HEPES (BioSolutions), pH 7.4, 10 mM $MgCl_2$, 0.005% Tween-20, 1.5 mM dithiothreitol (Pierce), 5 μg/mL leupeptin, 0.1 mM sodium orthovanadate (Alfa Aesar), 10 mM β-glycerophosphate, 2.5 mM EGTA, 1 mM NaF, 2% DMSO using 10−20 nM Plk. Apparent K_m, values were determined by varying ATP concentrations between 1 and 200 μM in assays containing 1.5 μCi γ^{33}P-ATP and 600 nM Cdc25c. Likewise, apparent $K_{m(CDC25c)}$ values were determined by varying Cdc25c concentrations between 1 and 3 μM at 200 μM ATP and 1.5 μCi γ^{33}P-ATP. Reactions were quenched at 5, 15, 30, 45, 60 min with 0.85% phosphoric acid. Phosphorylated product was captured on phosphocellulose membrane 96-well plate (Millipore MADPHNOB), washed with 0.85% phosphoric acid and counted on a Trilux microbeta scintillation counter. Unless mentioned otherwise, all reagents were from Sigma. Assays for Plk2 and Plk3 were performed using the Invitrogen SelectScreen kinase profiling service (Invitrogen Corporation, Carlsbad, CA). Activities against other kinases were determined as described (*49*).

Table 1: Data Collection and Refinement Statistics

dataset	AMPPNP	PHA-00680626
Data Collection		
space group	$P3_221$	$P3_221$
unit cell parameters (Å)	$a = b = 65.9$, $c = 153.9$	$a = b = 66.9$, $c = 153.6$
resolution (Å)	2.4	2.1
redundancy[a]	5.5 (4.0)	5.5 (3.9)
completeness (%)[a]	95.0 (79.5)	98.5 (89.3)
R_{merge}[a,b]	0.063 (0.344)	0.057 (0.263)
average I/σ[a]	9.2 (1.9)	9.4 (2.5)
Refinement		
no. reflections	14294	22445
no. test reflections	769	1205
R factor[c]	0.203	0.203
free *R* Factor	0.235	0.243
rms deviations		
bond lengths (Å)	0.009	0.006
bond angles (deg)	1.246	0.926
Average *B*-Factors (Å^2)		
all atoms	25.1	21.7
protein	22.8	18.7
inhibitor	83.5	33.1
acetate/Zn^{2+}/Mg^{2+}	45.9/44.6/42.1	52.1/47.0/−
waters	51.1	47.1
no. non-hydrogen atoms		
protein	2370	2387
inhibitor	31/44	32
waters	97	256
Ramachandran Plot Statistics		
% in most favored region	89.1	89.1
% additional allowed region	10.1	10.1
% generous allowed region	0.8	0.8

[a] Values in parentheses refer to the highest resolution shell. The two values for inhibitor non-hydrogen atoms for AMPPNP represent atoms for a single AMPPNP molecule and atoms including the alternative conformation observed, respectively. [b] $R_{merge} = \sum|I - \langle I\rangle| / \sum\langle I\rangle$. [c] *R* factor = $\sum||F_{obs}| - |F_{calc}||/\sum|F_{obs}|$ where F_{obs} and F_{calc} are the observed and calculated structure factors, respectively. Free *R* factor is calculated from a subset of reflections (5%) not used for refinement. The same subset was used for both datasets.

RESULTS AND DISCUSSION

Crystallization. Extensive screening of various constructs of human Plk1 (both with respect to construct boundaries and surface residue mutations to facilitate crystallization) was carried out without yielding crystals. However, this effort led to the identification of a fragment of Plk1 encompassing the entire kinase domain (residues 13−345, defined by limited proteolysis), which expressed well and was monodisperse as assessed by dynamic light scattering. Since this construct displayed favorable solution properties, and given the large number of constructs that had been tried without success, we decided to use it as the starting point for the design of expression constructs in which the primary phosphorylation site (Thr210) was mutated to either aspartate or valine with the aim of reducing conformational heterogeneity by stabilizing the activation loop in either an active or an inactive conformation, based on the observation that these mutations modulate Plk1 activity (*26*−*28*).

Initial screening of the Plk1 constructs was conducted by free interface diffusion using Fluidigm Topaz screening chips (*44*) and Fluidigm OptiMix crystallization screens. Using this setup, we obtained crystals of the T210V mutant Plk1 kinase domain. Extensive attempts to reproduce crystals in hanging drops were initially unsuccessful, and crystals were not reliably reproduced even in Topaz screening chips. We ultimately succeeded in obtaining diffraction-quality crystals in Topaz X-ray chips, which are designed to allow growth of larger crystals and extraction for diffraction analysis. The first structure solved revealed the presence of a divalent cation (Ni^{2+} or Zn^{2+}) involved in a crystal contact (see below). Addition of low levels of zinc acetate but not nickel sulfate or nickel chloride resulted in significantly more robust crystal growth during in-chip optimization, and inclusion of 0.3−0.6 mM Zn acetate in the reservoir solution ultimately allowed us to obtain crystals using the hanging drop method. We therefore suspect that serendipitous zinc from the Fluidigm crystallization buffers or screening chips was responsible for allowing Plk1 to crystallize in the chips. Subsequent experiments showed that the requirement for zinc is very narrow, as addition of 0.1 or 1 mM zinc acetate led to substantially fewer and smaller crystals during optimization. This low-level zinc requirement is usually not within the range of zinc concentrations in conventional screening buffers, providing a possible explanation why attempts to crystallize Plk1 by traditional screening methods were unsuccessful.

After optimizing crystallization of the T210V construct in hanging drops, we also succeeded in crystallizing the WT Plk1 kinase domain under similar conditions and in the same crystal form. However, WT crystals diffracted only to about 3 Å, leading us to focus on the mutant form. As outlined below, kinetic comparison between the different constructs indicates that the mutant structure can serve as a valid model for structure-based drug design. As with the wild-type construct, no crystal hits were obtained during initial screening of the T210D kinase domain. This protein expressed at lower levels than the other two constructs and was not pursued further.

Overall Structure of the Plk1 Kinase Domain. We solved the structures of the T210V mutant form of the Plk1 kinase domain in complex with the nonhydrolyzable ATP analogue AMPPNP or the pyrrolo-pyrazole inhibitor PHA-680626 (*42*) at 2.4 and 2.1 Å resolution, respectively (Figure 1, see Table 1 for data collection and refinement statistics). The structure displays the typical kinase fold in which the ATP binding site is located in a cleft formed between the N-terminal lobe (residues 37−131) composed predominantly of antiparallel β sheet and the primarily alpha-helical C-terminal lobe (residues 138−330). The two lobes are connected by a hinge region that makes conserved backbone interactions with the bound ligands. As both structures are very similar (rmsd = 0.41 Å for 276 equivalent alpha carbons), our analysis of the Plk1 structure is based on the higher resolution PHA-680626 structure, except when AMPPNP-specific features are discussed. There is continuous electron density for residues 37−330 with no density observed for residues 14−36 and 331−345. Residues 43−46 form an extra beta strand, preceding strand beta 1 of the kinase domain core as defined by Hanks and Hunter (*50*). Residues 306−330 are part of the linker connecting the kinase to the PBD domains. This segment is stabilized in an extended conformation by a crystal contact between Ile327 and a pocket in the back of the N-lobe of a symmetry-related Plk1 molecule (not shown). The general conformation of the kinase domain resembles that of active kinase structures, with an rmsd of 1.21 Å for 206 equivalent α-carbons between Plk1 and phosphorylated protein kinase A (PKA) (PDB ID 1ATP (*51*)). The alpha C helix is fully ordered, and the DFG motif, which defines the N-terminal anchor of the activation loop, is in the "DFG-in" conformation, where Phe195 is buried in a hydrophobic pocket and Asp194 is positioned for interactions with an active site Mg^{2+} and the phosphates of the nucleotide substrate. The orientations of other conserved active site residues also closely match those in other active kinases (Figure 1B).

Activation Loop. Although not phosphorylated, the activation loop of Plk1 (residues 194−221) is fully ordered and assumes an extended conformation similar to that of active kinase structures (*30*). The Zn^{2+} ion that proved to be critical for the crystallization of Plk1 mediates a crystal contact near the activation loop and is coordinated by Cys212 of the activation loop, His93 from the alpha C helix, Cys255 from the alpha G helix of a neighboring molecule and an acetate from the crystallization medium (Figure 1C). While the activation loop is in a conformation resembling that in active kinases, there are some features that are not compatible with an active conformation. When comparing the conformation of the activation loop of Plk1 to that of other kinases (e.g., PKA (*51*), PKB (*52*) or PDK1 (*53*)), the activation segment bulges around Cys212, presumably due to its interaction with the zinc ion, causing the P+1 loop of Plk1 to distort from the position it occupies in the active kinases (*30*). As a result, Thr214 of the P+1 loop is rotated outward relative from the position of the corresponding residue in active kinase structures and unable to form a hydrogen bond with Lys178 from the catalytic loop, an interaction that is conserved in the active states of Ser/Thr kinases (e.g., Thr201 and Lys168 in PKA, Figure 1C) (*54*). In addition to the disruption of this hydrogen bond, the conformation of Thr214 in our structure is likely incompatible with substrate binding, as indicated by an overlay of the substrate peptide from the active PKA structure onto the Plk1 structure, which shows a clash between the hydrophobic P+1 residue of the substrate (Ile in GSK3β, Leu in Cdc25c) and Thr 214 of Plk1 (Figure 1D). While it is possible that the observed active-like conformation of the activation loop is purely a crystallization artifact, we favor an explanation where both active and inactive conformations coexist in solution and the active conformation is selectively incorporated into growing crystals, where it is distorted to some extent by the interaction of Cys 212 with the zinc ion (see below).

Another residue apart from T210 in the activation loop that has been implicated in Plk1 activation is Ser137. Mutation of this residue to aspartate has been shown to increase the activity of Plk1 several fold (*27*, *28*), and distinct phenotypes have been observed in cell lines expressing the S137D and T210D mutant forms of Plk1 (*29*). Ser137 is located in a cleft at the transition from the hinge region to the alpha D helix (Figure 1A,D), and it is not obvious how this residue could be accessed by a phosphorylating kinase without significant conformational changes and/or movements of the two lobes of Plk1. As has been pointed out

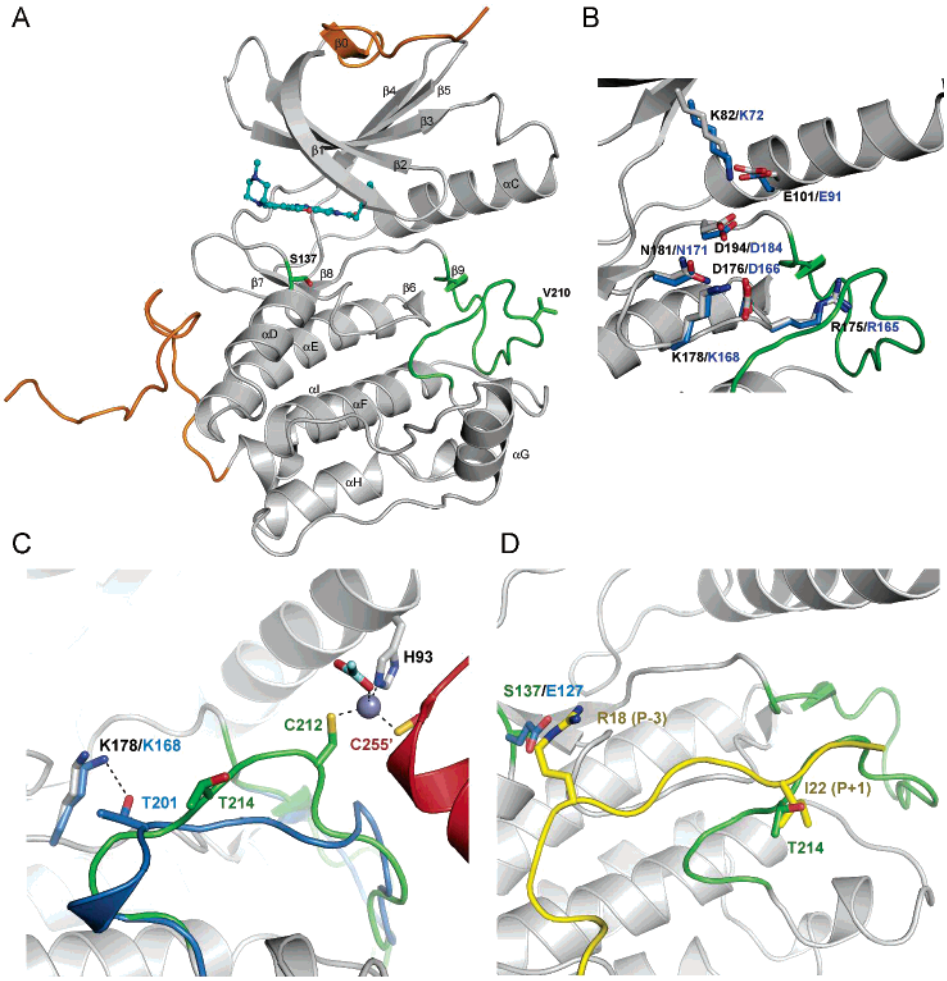

FIGURE 1: (A) Overview of the Plk1 kinase domain structure. Plk1 is shown in gray ribbon representation with N- and C-terminal extensions relative to the kinase domain core in orange and the activation loop in green. Residues Val210 in the activation loop (primary phosphorylation site Thr210 in WT Plk1) and Ser137 (proposed secondary phosphorylation site) are shown as green sticks. (B) Close up of the active site showing the orientation of conserved catalytic residues relative to PKA (PDB ID 1ATP, blue). Residue labels are color-coded. (C) Close-up of the area of the activation loop, highlighting the zinc-mediated crystal contact and distortions in the Plk1 activation loop relative to PKA. Coloring as in A. The alpha G helix of a symmetry-related Plk1 molecule participating in the crystal contact is shown as a red ribbon, and residues participating in the contact are shown as sticks. An acetate molecule that participates in the crystal contact is shown in light blue. The activation loop of PKA (PDB ID 1ATP) is overlaid in blue, with Thr201 and Lys168 shown as sticks to illustrate the interaction that is disrupted in Plk1 (residues Thr214 and Lys178). (D) Overlay of the PKA substrate peptide (PDB ID 1ATP, yellow) over the Plk1 structure with selected residues shown as sticks to highlight the clash of the P+1 residue with Plk1 Thr214 and interactions of the P-3 residue with Glu127 in PKA (Ser137 in Plk1). Residue labels are color coded. Figures were generated with Pymol (http://www.pymol.org).

elsewhere (*1*), this residue is positioned near the predicted P-3 position of bound protein substrates, and phosphorylation at this site could modulate Plk1 substrate specificity. The corresponding residue in PKA is a glutamate and interacts with the P-3 arginine in the PKA crystal structure (Figure 1D).

The ATP-Binding Pocket. The AMPPNP molecule is bound in a manner consistent with nucleotide binding in other kinases (Figure 2). The adenine portion is oriented in the binding site through hydrogen bonds between the backbone carbonyl of Glu131 and the C6 amino group of the inhibitor and between the Cys133 backbone amide and the N1 of the adenine ring. The face of the adenine ring system is sandwiched between Phe183 at the bottom of the binding site and Leu59, Cys67, and Ala80 in the roof of the pocket. The back of the adenine binding pocket is formed by the gatekeeper residue Leu130 and by Val114.

While the electron density map for the bound AMPPNP is easily interpreted in the region of the adenine and ribose, density for the phosphate groups is weak and they have been modeled in two alternative conformations guided by a $2F_o - F_c$ omit map. The ligand also displays significantly higher *B* factors than the rest of the protein (83.5 Å^2 for AMPPNP vs 22.8 Å^2 for protein atoms). The reason for the high flexibility of the phosphate groups revealed by the high *B* factors and alternate conformations is not immediately apparent from the structure but could be due in part to the fact that this region of the active site is not in a fully active conformation due to the zinc-mediated disruptions to the activation loop discussed above. Another possibility is that the high concentration (500 mM) of magnesium acetate in the crystallization buffer shields specific interactions of the phosphate groups of AMPPNP with the protein.

The PHA-680626 structure shows the inhibitor bound with the pyrrolo-pyrazole core oriented in a similar fashion to the adenine in AMPPNP and making equivalent hydrogen bonds with Glu131 and Cys133 of the hinge region (Figure 3C). An additional hydrogen bond that is often observed in

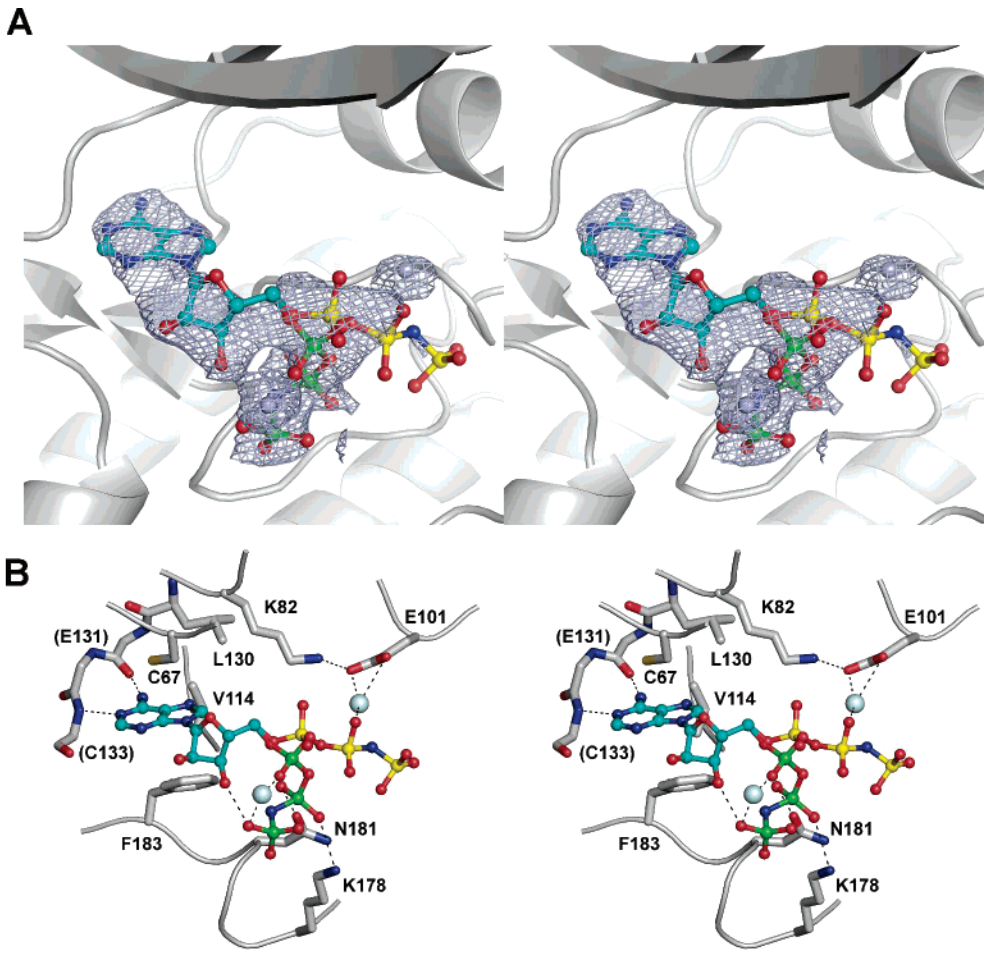

FIGURE 2: Binding mode of AMPPNP in Plk1. (A) $2F_o - F_c$ omit map contoured at 1 sigma for AMPPNP bound in the Plk1 active site (divergent stereoview). Both conformations of AMPPNP that were modeled into the electron density are shown superimposed with the phosphates in yellow and green, respectively. Density for the gamma-phosphate group in the extended conformation is poor but is more evident at contour levels slightly lower than 1 sigma and could reflect increased flexibility of this group in the extended conformation. (B) Divergent stereoview of the AMPPNP binding mode showing both modeled conformations for the phosphate groups. Magnesium ions are represented as light blue spheres. Main chain atoms are omitted, except for residues in the hinge region. Side chains are not shown for residues labeled in parentheses.

kinase−inhibitor complexes is formed between the amide linker and the backbone carbonyl of Cys133. This orientation positions the inhibitor in such a way that the methylpiperazine is pointing out into solvent and the thiophene ring is positioned in the binding site. In contrast to the AMPPNP structure, the *B* factors for PHA-680626 are only moderately higher than those for the protein (33.1 and 18.7 Å^2, respectively), and the density for the ligand is well defined. The binding mode of PHA-680626 in Plk1 is similar to that of the related compound PHA-680632 in Aurora A (*42*) (Figure 3D). Apart from the interactions with the hinge region, PHA-680626 makes water-mediated hydrogen bonds with Lys82 and His105 in the back of the binding pocket. Probably owing to the presence of Arg136, the methylpiperazine portion of the inhibitor is oriented perpendicular to the plane of the phenyl ring and pointing toward the N-terminal lobe, rather than extending straight into solvent as observed for PHA-680632 in the Aurora A structure.

Kinetic Characterization and Validation of Structure. To understand why the T210V mutant Plk1 crystallized in a conformation similar to that of active kinases, as well as to validate the utility of the T210V structure for structure-based drug design, kinetic characterization of the WT, T210D, and T210V kinase domain constructs was carried out (Table 2). All constructs display essentially unchanged apparent K_m values for both ATP and the protein substrate. As has been shown previously for mutations of the primary phosphorylation site (*26*−*28*), the specific activity of Plk1 is increased for the T210D mutant relative to WT and reduced but not abolished for T210V. Using the values obtained with ATP as the constant substrate, we observed an approximately 4-fold activation relative to WT for T210D and a 2-fold reduction in activity for T210V. The residual kinase activity for the T210V mutant confirms that this construct is capable of adopting a conformation that is catalytically competent. It should be pointed out that the WT Plk1 kinase domain analyzed here is unphosphorylated as determined by mass spectrometry and as such would be expected to have kinetic parameters similar to the T210V mutant.

We next determined IC_{50} values for AMPPNP and PHA-680626 for the WT and mutant kinase domain constructs (Table 3) and found little effect of the activation loop mutations on the potency of these compounds. Similar results were observed for several other inhibitors that displayed a range of potencies against Plk1 (not shown). These findings

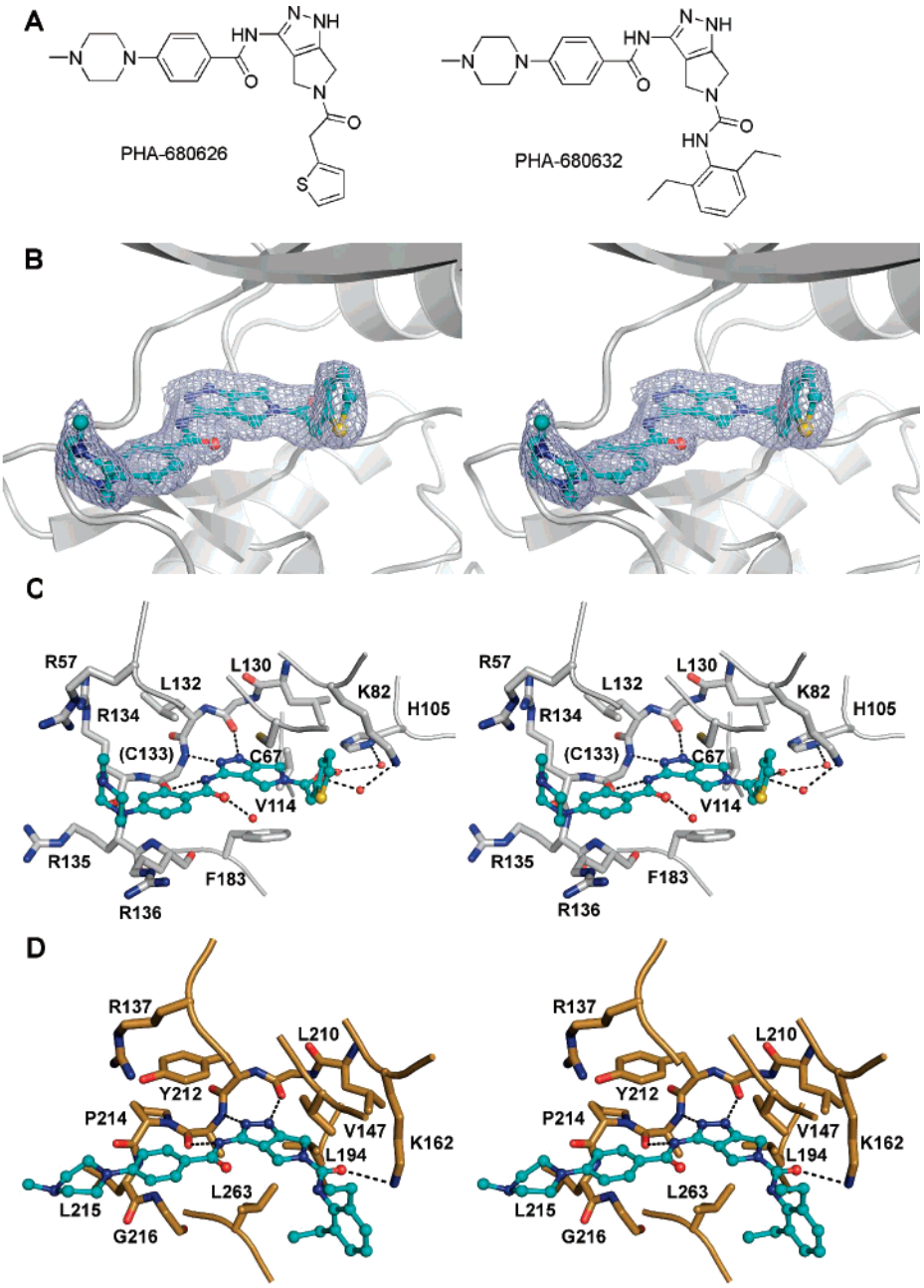

FIGURE 3: Binding mode of pyrrolo-pyrazole inhibitors in Plk1 and Aurora A. (A) Chemical structure of PHA-680626 and PHA-680632. (B) $2F_o - F_c$ omit map contoured at 1 sigma for PHA-680626 bound to Plk1. (C) Divergent stereoview of the binding mode of PHA-680626 bound to Plk1. Residues without side chain representations are labeled in parentheses. (D) Divergent stereoview of PHA-680632 bound to Aurora A (PDB ID 2BMC).

Table 2: Kinetic Parameters for Plk Kinase Domain (KD) Constructs[a]

Plk1	varied substrate	constant substrate	K_m (μM)	k_{cat} (s^{-1})	k_{cat}/K_m ($M^{-1}\,s^{-1}$)
WT	ATP	Cdc25c[b]	3.2 ± 1.4	0.0041 ± 0.0017	1.3×10^3
	Cdc25c	ATP	0.66 ± 0.16	0.0094 ± 0.0009	1.4×10^4
T210D	ATP	Cdc25c[b]	4.0 ± 1.2	0.0190 ± 0.0050	4.8×10^3
	Cdc25c	ATP	0.60 ± 0.14	0.0376 ± 0.0014	6.3×10^4
T210V	ATP	Cdc25c[b]	3.0 ± 0.4	0.0019 ± 0.0003	0.6×10^3
	Cdc25c	ATP	0.80 ± 0.02	0.0049 ± 0.0001	0.6×10^4

[a] All values represent the average of two measurements; standard errors are indicated. [b] Presence of subsaturating concentrations of Cdc25C (0.6 μM).

are consistent with the observation that the ATP apparent K_m is very similar for the three constructs and shows that the mutations at position 210 do not influence binding of ATP or ATP-competitive inhibitors to an appreciable extent. This finding suggests that the structure is a valid tool to guide structure-based drug design and that interpretations with respect to ligand binding based on the T210V kinase domain structure may be translated to the WT protein.

It is interesting that the least active of the three constructs crystallized most readily and that it did so in an active-like

Table 3: IC_{50} Values (μM) for WT, T210D, and T210V Plk1 Kinase Domain Constructs[a]

ligand	WT	T210D	T210V
AMPPNP	166 ± 38	140 ± 29	155 ± 64
PHA-680626	0.53 ± 0.14	0.34 ± 0.10	0.44 ± 0.12

[a] All values represent the average of three measurements; standard errors are indicated.

conformation, contradicting our rationale of stabilizing an inactive conformation with the T210V mutation. A possible explanation is that, as generally believed for kinases, the active and inactive conformations exist in equilibrium in solution for all three constructs and that our crystallization condition prefers crystal packing of the active-like conformation. Even though the T210D construct would be expected to populate this conformation more readily and therefore crystallize more easily, valine at position 210 might be preferred for crystallization in the current crystal form over threonine or aspartate, resulting in enrichment of the active-like conformation in the crystals, even though this conformation might only constitute a minor fraction of the molecules in solution.

While mutations of Thr210 in Plk1 have been shown to change Plk1 kinase activity and affect Plk1 function in vivo, regulation of Plk1 in the cellular context also relies on interactions of the PBD with the kinase domain and with interacting partners, as well as changing protein levels throughout the cell cycle. It is therefore possible that the activation loop conformation does not need to be as tightly controlled in Plk1 as in other kinases and that a large enough fraction of the T210V protein exists in an active conformation in solution to allow its selection for incorporation into crystals. In kinases where the catalytic aspartate is preceded by an invariant arginine (RD-kinases), this arginine contributes to a basic patch on the protein surface that helps neutralize the charge of the phosphorylated activation loop and stabilizes the active conformation of the kinase (RD-pocket) (*54*). Two of the residues that contribute to the RD pocket are not conserved in Plk1 (Met100 and Thr199, corresponding to Asn90 and Lys189 in PKA). This could result in a reduced amount of electrostatic repulsion within the RD pocket in unphosphorylated Plk1 and allow for the active state to be populated more frequently than in other kinases.

Implications for Selectivity. To identify areas of the Plk1 active site that are important for selectivity against other kinases, we compared the potency of PHA-680626 against a number of serine/threonine and tyrosine kinases (Table 4). Plk1, Plk2, Aurora A, fibroblast growth factor receptor 1 (FGFR1), vascular endothelial growth factor receptor 3 (VEGFR3) and Abelson tyrosine kinase (ABL) are inhibited at sub-micromolar potencies, with weaker inhibition detected against Plk3, CDK2, glycogen synthase kinase 3 beta (GSK3β), and CHK1. The compound shows an approximately 10-fold selectivity for Aurora A over Plk1. This modest difference in potency is probably explained in part by the presence of Phe183 at the bottom of the Plk1 binding site, which restricts the available conformations of the thiophene portion of PHA-680626 relative to Aurora A, where the corresponding residue is a leucine (see Figure 3D and sequence alignment in Figure 4). Owing to the bulk of

Table 4: Selectivity Profile for PHA-680626[a]

kinase	PHA-680626 IC50 (μM)	S.D.
Plk1	0.53	± 0.14 (n = 3)
Plk2	0.07	± 0.01 (n = 4)
Plk3	1.61	± 0.36 (n = 6)
Aurora A	0.07	± 0.02 (n = 4)
FGFR1	0.12	± 0.04 (n = 2)
VEGFR3	0.38	± 0.18 (n = 2)
ABL	0.89	± 0.10 (n = 2)
CDK2/CYCA	2.0	± 0.30 (n = 3)
GSK3β	2.57	± 0.31 (n = 3)
CHK1	4.95	± 0.35 (n = 2)
EGFR1	>10	(n = 1)
IRK	>10	(n = 1)
LCK	>10	(n = 1)
LYN	>10	(n = 1)
NIM1	>10	(n = 1)
PKC beta	>10	(n = 1)
PKAα	>10	(n = 1)

[a] The potency of PHA-680626 for Plk1 was determined as described in Materials and Methods. Assays for Plk2 and Plk3 were performed using the Invitrogen SelectScreen kinase profiling service. Selectivity data for kinases other than the Plks were extracted from an internal database. Assays for these kinases were performed as described in ref *49*. The average of multiple determinations and the standard deviation are shown where applicable.

Phe183, the thiophene of the inhibitor in the Plk1 structure points to the roof of the active site, where the presence of the smaller Cys67 in Plk1 instead of valine in most of the other tested kinases creates the space to accommodate this conformation of the inhibitor. It is expected that the combination of valine in the roof of the pocket and the less bulky (relative to phenylalanine) leucine or methionine at the bottom of the pocket forces the inhibitor to bind in an alternate conformation with the thiophene pointing down in Aurora A and other kinases. The presence in NIM1 of Phe203 in the position corresponding to Phe183 in Plk1, together with the relatively bulky leucine compared to Cys67, is expected to prevent binding of PHA-680626 in either conformation, explaining the lack of potency for this compound. The lack of activity against the AGC kinases PKA and PKC beta can probably be explained by their C-terminal extension relative to the kinase core that wraps around the front of the active site and allows the hydrophobic motif (HM) to interact with the HM-binding pocket at the back of the N-lobe (*51*). This segment is predicted to clash with the solvent-exposed methylpiperazine of the inhibitor. In addition to creating extra space in the binding site, the presence of Cys67 in the roof of the Plk1 binding pocket also provides an opportunity to exploit the special character of this reactive residue for the design of covalent inhibitors, as has been demonstrated for the equivalent residue in the C-terminal kinase domain of RSK1 and RSK2 (*55*).

Given that the valine/leucine pair occurs both in kinases that are sensitive to PHA-680626, as well as in those that do not show inhibition, other parts of the binding site have to be important for selectivity. One area of interest in this regard is the region around the solvent-exposed methylpiperazine of the inhibitor, where there is an unusual concentration of positively charged side chains in Plk1: Arg134, Arg135, Arg136, and Arg57. Of these, only Arg57 is moderately conserved as either arginine or lysine, while

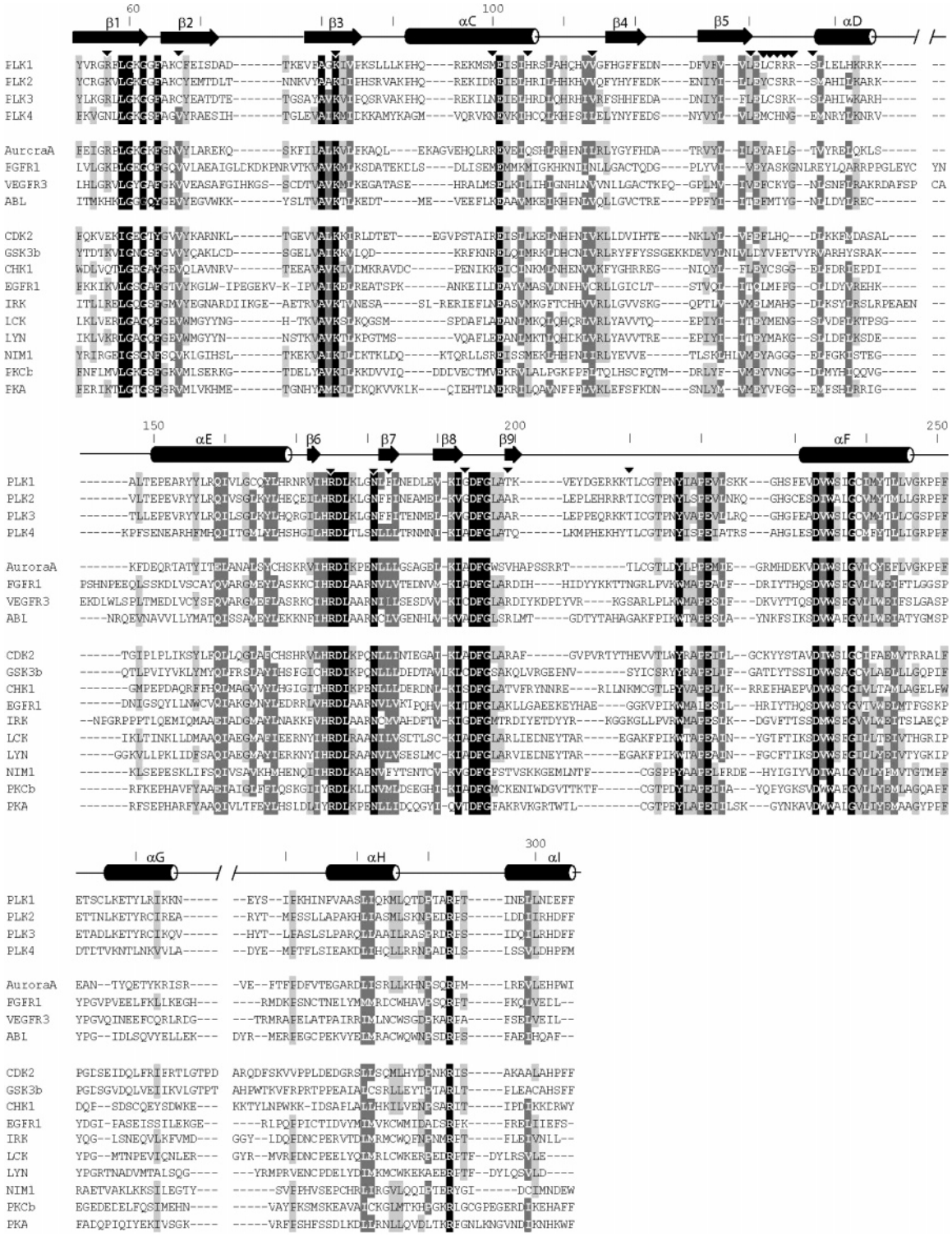

FIGURE 4: Alignment of the kinase domains of selected serine/threonine and tyrosine kinases. The secondary structures and residue numbers for the Plk1 kinase domain are indicated (note that the N- and C-terminal extensions in the Plk1 structure relative to the kinase core are not covered in this alignment). Invariant and conserved residues are highlighted in black and gray, respectively. Insertions in FGFR1, VEGFR3, CDK2, and GSK3β are truncated as indicated by the parallel slash marks on the secondary structure schematic. Plk1 residues discussed in the text are marked by black triangles.

Arg136 is a very unusual residue at this position which is frequently a glycine in other kinases. Differences in the number of positively charged side chains in this area in other kinases would be expected to change the interaction with the solvent-exposed part of the inhibitor.

The Plk1 inhibitor BI 2536 was demonstrated to inhibit Plk1 with greater than 10000-fold selectivity versus 43 other kinases tested (*35*). Docking of this inhibitor into Plk1 reveals several features that might be important for its high selectivity (Figure 5). The ortho-methoxy group of the phenyl substituent of the inhibitor occupies a pocket created by the presence of Leu132 in the Plk1 hinge region at a position that is generally conserved as either tyrosine or phenylalanine in other kinases. It is unlikely that BI 2536 could bind in

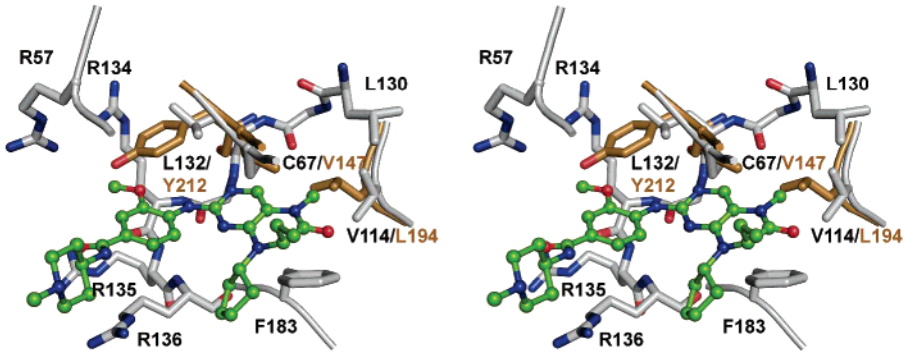

FIGURE 5: Proposed binding mode for the selective Plk1 inhibitor BI 2536 in Plk1. Docking was performed using an internally developed docking program which allows for compound flexibility but keeps the protein rigid. The compound is positioned with the methoxy group of the inhibitor in the selectivity pocket formed by the presence in Plk1 of Leu132 compared to the bulkier tyrosine or phenylalanine in many other kinases. The methyl and ethyl substituents of the pteridinone core are positioned close to Val114 and Cys67, respectively, and might also contribute to the reported selectivity of this inhibitor. Residues from Aurora A (PDB ID 2BMC) are overlaid in brown.

the proposed orientation to kinases with the bulkier amino acids at this position. The ethyl substituent of the inhibitor is located near Cys67 in the roof of the binding site. This group might not be accommodated easily in other kinases where the corresponding residue frequently is a valine. Finally, the methyl substituent of the pteridinone core points toward Val114 positioned below the gatekeeper residue L130 and might not be tolerated in kinases where the corresponding residue is more bulky, like Leu194 in Aurora A.

For the design of specific Plk1 inhibitors, selectivity against other Plk isoforms is also desirable. While Plk2, 3, and 4 share similar sequence identity with Plk1 across the kinase domain (32, 25, and 34% identity, respectively), examination of residues expected to be important for inhibitor binding from the alignment in Figure 4 shows that Plk2 and Plk3 are more similar to Plk1 in this respect than is Plk4. The cysteine/phenylalanine pair that characterizes the roof and bottom of the Plk1 nucleotide binding site is conserved in Plk2 and Plk3, but in Plk4 these residues are the more commonly occurring valine and leucine. Plk4 also does not contain any of the three arginine residues in the hinge region (Arg134−136 in Plk1), while Plk2 and Plk3 each contain two basic residues in this area. Furthermore, Plk4 is the only Plk isoform that has a negatively charged glutamate residue in place of Ser137 in Plk1. In agreement with the observation that Plk2 and Plk3 display few differences in residues interacting with the inhibitor compared to Plk1, PHA-680626 exhibits similar potencies against these kinases (Table 4). Selectivity against Plk2 could be achieved by targeting the pocket created by Leu132 in Plk1, which is predicted to not be present in Plk2, where the corresponding residue is the more commonly observed tyrosine.

CONCLUSIONS

In summary, we report the crystal structures of the Plk1 kinase domain complexed with AMPPNP or the Aurora A kinase inhibitor PHA-680626. The structures reveal the typical kinase fold with the unphosphorylated (T210V) activation loop in an extended conformation, stabilized by a crystal contact. Kinetic characterization of WT and mutant kinase domain constructs demonstrates that while the T210V mutation results in lower kinase activity it does not affect substrate or ATP apparent K_m or IC_{50} values for the tested inhibitors. Unique features of the Plk1 ATP binding site that provide opportunities for the design of potent and selective inhibitors include the presence of a bulky phenylalanine at the bottom of the binding site combined with a smaller cysteine in the roof of the pocket that is a valine in many other kinases, a pocket created by Leu132 in the hinge region, and a cluster of positively charged residues in the solvent-exposed area outside of the adenine pocket.

ACKNOWLEDGMENT

We thank Leyu Wang for help in construct generation, Yan Zhang for mass spectrometry analysis, Andy May from Fluidigm for help with crystal optimization and extraction from X-ray chips, and Ralph Lambalot, Steven Faraci, Ajith Kamath, Daniel Caffrey, and Jessie English for helpful discussions.

REFERENCES

1. Lowery, D. M., Lim, D., and Yaffe, M. B. (2005) Structure and function of Polo-like kinases, *Oncogene 24*, 248−259.
2. Barr, F. A., Sillje, H. H., and Nigg, E. A. (2004) Polo-like kinases and the orchestration of cell division, *Nat. Rev. Mol. Cell Biol. 5*, 429−440.
3. Strebhardt, K., and Ullrich, A. (2006) Targeting polo-like kinase 1 for cancer therapy, *Nat. Rev. Cancer 6*, 321−330.
4. Holtrich, U., Wolf, G., Brauninger, A., Karn, T., Bohme, B., Rubsamen-Waigmann, H., and Strebhardt, K. (1994) Induction and down-regulation of PLK, a human serine/threonine kinase expressed in proliferating cells and tumors, *Proc. Natl. Acad. Sci. U.S.A. 91*, 1736−1740.
5. Dietzmann, K., Kirches, E., von Bossanyi, P., Jachau, K., and Mawrin, C. (2001) Increased human polo-like kinase-1 expression in gliomas, *J. Neurooncol. 53*, 1−11.
6. Takai, N., Miyazaki, T., Fujisawa, K., Nasu, K., Hamanaka, R., and Miyakawa, I. (2001) Expression of polo-like kinase in ovarian cancer is associated with histological grade and clinical stage, *Cancer Lett. 164*, 41−49.
7. Takahashi, T., Sano, B., Nagata, T., Kato, H., Sugiyama, Y., Kunieda, K., Kimura, M., Okano, Y., and Saji, S. (2003) Polo-like kinase 1 (PLK1) is overexpressed in primary colorectal cancers, *Cancer Sci. 94*, 148−152.
8. Knecht, R., Elez, R., Oechler, M., Solbach, C., von Ilberg, C., and Strebhardt, K. (1999) Prognostic significance of polo-like kinase (PLK) expression in squamous cell carcinomas of the head and neck, *Cancer Res. 59*, 2794−2797.
9. Wolf, G., Elez, R., Doermer, A., Holtrich, U., Ackermann, H., Stutte, H. J., Altmannsberger, H. M., Rubsamen-Waigmann, H., and Strebhardt, K. (1997) Prognostic significance of polo-like

kinase (PLK) expression in non-small cell lung cancer, *Oncogene 14*, 543−549.
10. Tokumitsu, Y., Mori, M., Tanaka, S., Akazawa, K., Nakano, S., and Niho, Y. (1999) Prognostic significance of polo-like kinase expression in esophageal carcinoma, *Int. J. Oncol. 15*, 687−692.
11. Kneisel, L., Strebhardt, K., Bernd, A., Wolter, M., Binder, A., and Kaufmann, R. (2002) Expression of polo-like kinase (PLK1) in thin melanomas: a novel marker of metastatic disease, *J. Cutan. Pathol. 29*, 354−358.
12. Lane, H. A., and Nigg, E. A. (1996) Antibody microinjection reveals an essential role for human polo-like kinase 1 (Plk1) in the functional maturation of mitotic centrosomes, *J. Cell Biol. 135*, 1701−1713.
13. Spankuch-Schmitt, B., Wolf, G., Solbach, C., Loibl, S., Knecht, R., Stegmuller, M., von Minckwitz, G., Kaufmann, M., and Strebhardt, K. (2002) Downregulation of human polo-like kinase activity by antisense oligonucleotides induces growth inhibition in cancer cells, *Oncogene 21*, 3162−3171.
14. Liu, X., and Erikson, R. L. (2003) Polo-like kinase (Plk)1 depletion induces apoptosis in cancer cells, *Proc. Natl. Acad. Sci. U.S.A. 100*, 5789−5794.
15. Guan, R., Tapang, P., Leverson, J. D., Albert, D., Giranda, V. L., and Luo, Y. (2005) Small interfering RNA-mediated Polo-like kinase 1 depletion preferentially reduces the survival of p53-defective, oncogenic transformed cells and inhibits tumor growth in animals, *Acta Crystallogr. D. Biol. Crystallogr. 65*, 2698−2704.
16. Elez, R., Piiper, A., Kronenberger, B., Kock, M., Brendel, M., Hermann, E., Pliquett, U., Neumann, E., and Zeuzem, S. (2003) Tumor regression by combination antisense therapy against Plk1 and Bcl-2, *Oncogene 22*, 69−80.
17. Elia, A. E., Rellos, P., Haire, L. F., Chao, J. W., Ivins, F. J., Hoepker, K., Mohammad, D., Cantley, L. C., Smerdon, S. J., and Yaffe, M. B. (2003) The molecular basis for phosphodependent substrate targeting and regulation of Plks by the Polo-box domain, *Cancer Sci. 115*, 83−95.
18. Cheng, K. Y., Lowe, E. D., Sinclair, J., Nigg, E. A., and Johnson, L. N. (2003) The crystal structure of the human polo-like kinase-1 polo box domain and its phospho-peptide complex, *EMBO J. 22*, 5757−5768.
19. Lee, K. S., Grenfell, T. Z., Yarm, F. R., and Erikson, R. L. (1998) Mutation of the polo-box disrupts localization and mitotic functions of the mammalian polo kinase Plk, *Proc. Natl. Acad. Sci. U.S.A. 95*, 9301−9306.
20. Elia, A. E., Cantley, L. C., and Yaffe, M. B. (2003) Proteomic screen finds pSer/pThr-binding domain localizing Plk1 to mitotic substrates, *Science 299*, 1228−1231.
21. Mundt, K. E., Golsteyn, R. M., Lane, H. A., and Nigg, E. A. (1997) On the regulation and function of human polo-like kinase 1 (PLK1): effects of overexpression on cell cycle progression, *Biochem. Biophys. Res. Commun. 239*, 377−385.
22. Jang, Y. J., Lin, C. Y., Ma, S., and Erikson, R. L. (2002) Functional studies on the role of the C-terminal domain of mammalian polo-like kinase, *Proc. Natl. Acad. Sci. U.S.A. 99*, 1984−1989.
23. Golsteyn, R. M., Schultz, S. J., Bartek, J., Ziemiecki, A., Ried, T., and Nigg, E. A. (1994) Cell cycle analysis and chromosomal localization of human Plk1, a putative homologue of the mitotic kinases Drosophila polo and Saccharomyces cerevisiae Cdc5, *J. Cell Sci. 107 (Pt 6)*, 1509−1517.
24. Cheng, L., Hunke, L., and Hardy, C. F. (1998) Cell cycle regulation of the Saccharomyces cerevisiae polo-like kinase cdc5p, *Mol. Biol. Cell 18*, 7360−7370.
25. Lindon, C., and Pines, J. (2004) Ordered proteolysis in anaphase inactivates Plk1 to contribute to proper mitotic exit in human cells, *J. Cell Biol. 164*, 233−241.
26. Lee, K. S., and Erikson, R. L. (1997) Plk is a functional homolog of Saccharomyces cerevisiae Cdc5, and elevated Plk activity induces multiple septation structures, *Mol. Cell Biol. 17*, 3408−3417.
27. Qian, Y. W., Erikson, E., and Maller, J. L. (1999) Mitotic effects of a constitutively active mutant of the Xenopus polo-like kinase Plx1, *Mol. Cell Biol. 19*, 8625−8632.
28. Jang, Y. J., Ma, S., Terada, Y., and Erikson, R. L. (2002) Phosphorylation of threonine 210 and the role of serine 137 in the regulation of mammalian polo-like kinase, *J. Biol. Chem. 277*, 44115−44120.
29. van de Weerdt, B. C., van Vugt, M. A., Lindon, C., Kauw, J. J., Rozendaal, M. J., Klompmaker, R., Wolthuis, R. M., and Medema, R. H. (2005) Uncoupling anaphase-promoting complex/cyclosome activity from spindle assembly checkpoint control by deregulating polo-like kinase 1, *Mol. Cell. Biol. 25*, 2031−2044.
30. Nolen, B., Taylor, S., and Ghosh, G. (2004) Regulation of protein kinases: Controlling activity through activation segment conformation, *Mol. Cell 15*, 661−675.
31. McInnes, C., Mezna, M., and Fischer, P. M. (2005) Progress in the discovery of polo-like kinase inhibitors, *Curr. Top. Med. Chem. 5*, 181−197.
32. Stevenson, C. S., Capper, E. A., Roshak, A. K., Marquez, B., Eichman, C., Jackson, J. R., Mattern, M., Gerwick, W. H., Jacobs, R. S., and Marshall, L. A. (2002) The identification and characterization of the marine natural product scytonemin as a novel antiproliferative pharmacophore, *J. Pharmacol. Exp. Ther. 303*, 858−866.
33. Liu, Y., Shreder, K. R., Gai, W., Corral, S., Ferris, D. K., and Rosenblum, J. S. (2005) Wortmannin, a widely used phosphoinositide 3-kinase inhibitor, also potently inhibits mammalian polo-like kinase, *Chem. Biol. 12*, 99−107.
34. Walker, E. H., Pacold, M. E., Perisic, O., Stephens, L., Hawkins, P. T., Wymann, M. P., and Williams, R. L. (2000) Structural determinants of phosphoinositide 3-kinase inhibition by wortmannin, LY294002, quercetin, myricetin, and staurosporine, *Mol. Cell 6*, 909−919.
35. Steegmaier, M., Baum, A., Solca, F., Peters, J. M., Grauert, M., and Hoffmann, M. (2005) BI 2536, a potent and highly selective inhibitor of Polo-like kinase 1 (Plk1), induces mitotic arrest and apoptosis in a broad spectrum of tumor cell lines, *Clin. Cancer Res. 11* (Suppl.), 9147.
36. Baum, A., Garin-Chesa, P., Quant, J., Colbatzky, F., Munzert, G., Grauert, M., Hoffmann, M., and Steegmaier, M. (2005) In vivo activity of BI 2536, a potent and selective inhibitor of the mitotic kinase Plk1, in a range of human cancer xenograft models, *Clin. Cancer Res. 11* (Suppl.), 9146.
37. Mross, K., Steinbild, S., Frost, A., Hedborn, S., Rentschler, J., Kaiser, D., Trommeshauser, D., Stehle, G., and Munzert, G. (2005) A Phase I single dose escalation study of the Polo-like kinase 1 inhibitor BI 2536 in patients with advanced solid tumors, *Clin. Cancer Res. 11* (Suppl.), 9032.
38. McInnes, C., Meades, C., Mezna, M., and Fischer, P. (2004) PCT Int. Pat. Appl. Publ. WO 2004067000.
39. Umehara, H., Yamashita, Y., Tsujita, T., Arai, H., Hagihara, K., and Machii, D. (2004) PCT Int. Pat. Appl. Publ. WO 2004043936.
40. Davis-Ward, R., Mook, R. A. J., Neeb, M. J., and Salovich, J. M. (2004) PCT. Int. Pat. Appl. Publ. WO 2004074244.
41. Andrews, C. W., III, Cheung, M., Davis-Ward, R. G., Drewry, D. H., Emmitte, K. A., Hubbard, R. D., Kuntz, K. W., Linn, J. A., Mook, R. A., Smith, G. K., and Veal, J. M. (2004) PCT Int. Pat. Appl. Publ. WO 2004014899.
42. Fancelli, D., Berta, D., Bindi, S., Cameron, A., Cappella, P., Carpinelli, P., Catana, C., Forte, B., Giordano, P., Giorgini, M. L., Mantegani, S., Marsiglio, A., Meroni, M., Moll, J., Pittala, V., Roletto, F., Severino, D., Soncini, C., Storici, P., Tonani, R., Varasi, M., Vulpetti, A., and Vianello, P. (2005) Potent and selective Aurora inhibitors identified by the expansion of a novel scaffold for protein kinase inhibition, *J. Med. Chem. 48*, 3080−3084.
43. Wasilko, D. J., and Lee, S. E. (2006) TIPS: Titerless infected-cells preservation and scale-up, *BioProcess. J. 5*, 29−32.
44. Segelke, B. (2005) Macromolecular crystallization with microfluidic free-interface diffusion, *Expert Rev. Proteomics 2*, 165−172.
45. Otinowski, Z., and Minor, W. (1997) Processing of X-ray diffraction data collected in oscillation mode, *Methods Enzymol. 276*, 307−326.
46. Collaborative Computational Project, Number 4. (1994) The CCP4 suite: programs for protein crystallography, *Acta Crystallogr. D. Biol. Crystallogr. 50*, 760−763.
47. Murshudov, G. N., Vagin, A. A., and Dodson, E. J. (1997) Refinement of macromolecular structures by the maximum-likelihood method, *Acta Crystallogr. D. Biol. Crystallogr. 53*, 240−255.
48. Oldfield, T. J., and Hubbard, R. H. (1994) Analysis of Cα geometry in protein structures, *Protein: Struct., Funct. Genet. 18*, 324−337.
49. Pevarello, P., Brasca, M. G., Amici, R., Orsini, P., Traquandi, G., Corti, L., Piutti, C., Sansonna, P., Villa, M., Pierce, B. S., Pulici, M., Giordano, P., Martina, K., Fritzen, E. L., Nugent, R. A., Casale, E., Cameron, A., Ciomei, M., Roletto, F., Isacchi, A., Fogliatto, G., Pesenti, E., Pastori, W., Marsiglio, A., Leach, K.

L., Clare, P. M., Fiorentini, F., Varasi, M., Vulpetti, A., and Warpehoski, M. A. (2004) 3-Aminopyrazole inhibitors of CDK2/cyclin A as antitumor agents. 1. Lead finding, *J. Med. Chem. 47*, 3367−3380.

50. Hanks, S., and Hunter, T. (1995) Protein kinases 6. The eukaryotic protein kinase superfamily: kinase (catalytic) domain structure and classification, *FASEB J. 9*, 576−596.
51. Zheng, J., Knighton, D. R., ten Eyck, L. F., Karlsson, R., Xuong, N., Taylor, S. S., and Sowadski, J. M. (1993) Crystal structure of the catalytic subunit of cAMP-dependent protein kinase complexed with MgATP and peptide inhibitor, *Biochemistry 32*, 2154−2161.
52. Yang, J., Cron, P., Good, V. M., Thompson, V., Hemmings, B. A., and Barford, D. (2002) Crystal structure of an activated Akt/Protein Kinase B ternary complex with GSK3-peptide and AMP-PNP, *Nat. Struct. Biol. 9*, 940−944.
53. Biondi, R. M., Komander, D., Thomas, C. C., Lizcano, J. M., Deak, M., Alessi, D. R., and van Aalten, D. M. F. (2002) High resolution crystal structure of the human PDK1 catalytic domain defines the regulatory phosphopeptide docking site, *EMBO J. 21*, 4219−4228.
54. Krupa, A., Preethi, G., and Srinivasan, N. (2004) Structural modes of stabilization of permissive phosphorylation sites in protein kinases: Distinct strategies in Ser/Thr and Tyr kinases, *J. Mol. Biol. 339*, 1025−1039.
55. Cohen, M. S., Zhang, C., Shokat, K. M., and Taunton, J. (2005) Structural bioinformatics-based design of selective, irreversible kinase inhibitors, *Science 308*, 1318−1321.

BI602474J